RSC Advances

ROYAL SOCIETY OF CHEMISTRY

www.rsc.org/advances

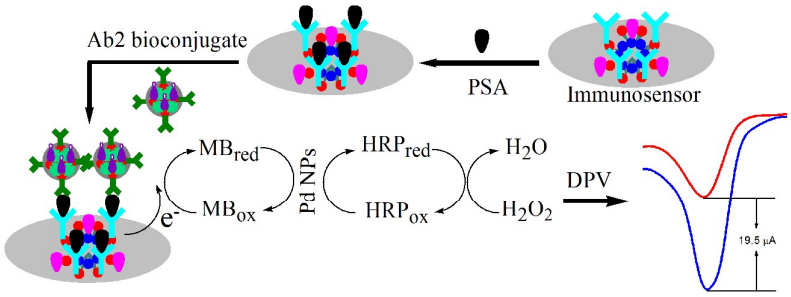

Graphic Abstract

The illustration for the constructed electrochemical immunosensor and the signal amplification strategy.

Immunosensor for prostate-specific antigen using Au/Pd@flower-like SnO_2 as platform and Au@mesoporous carbon as signal amplification

Long Yang[a, 1], Hui Zhao[b, 1], Guogang Deng[a], Xin Ran[a], Yucong Li[a], Xiaoguang Xie[a], Can-Peng Li[a,*]

[a] School of Chemical Science and Technology, Yunnan University, Kunming 650091, PR China.

[b] Laboratory for Conservation and Utilization of Bio-resource, Yunnan University, Kunming 650091, PR China.

[1]These authors contributed equally to this work.

* Corresponding author.

Fax or Tel: 86-871-65031119. E-mail: lcppp1974@sina.com (C.-P. Li)

Abstract: In the present work, a sandwich-type electrochemical immunosensor for ultrasensitive determination of prostate-specific antigen (PSA) was designed by using Au/Pd@SnO_2 as sensing platform and gold@mesoporous carbon nanocomposites (Au@CMK-3) as signal amplification. In this work, Au@CMK-3 was prepared for immobilizing plentiful of redox probe-methylene blue (MB), horseradish peroxidase (HRP), and secondary antibodies (Ab2), leading to the formation of Au@CMK-3-MB-Ab2-HRP bioconjugate. Furthermore, Au/Pd@SnO_2 was utilized as the biosensor platform to immobilize the primary antibodies (Ab1) leading a further enhancement in the sensitivity of immunosensor. With the synergistic effects among the Au/Pd@SnO_2 platform, the Au@CMK-3 nanocarrier, the ultrafine Pd NPs electrocatalyst, and HRP enzymatic reactions, almost double amplified detection signal was achieved in the presence of H_2O_2, so as to improve the detection limit of the proposed immunosensor effectively. The constructed immunosensor exhibited desirable performance for determination of PSA with a wide linearity in the range from 0.01 to 100 ng mL^{-1} and a relatively low detection limit of 3 pg mL^{-1}. The proposed immunosensor was also used to determine PSA in human serum with satisfactory results, implying potential applications in immunoassays.

1. Introduction

Immunosensors based on antibody–antigen binding are one of the most widely used sensors to detect disease related substances, which are known as biomarkers, in clinical diagnostics. [1] Highly sensitive detection and accurate analysis of biomarker

molecules in human fluid samples are essential for early detection, treatment and management of cancer. [2] Prostate cancer is a common malignancy and is one of the top 10 leading causes of cancer deaths in the male population. [3] Prostate specific antigen (PSA) is the best serum marker currently available for the preoperative diagnosis and screening of prostate cancer. [4] It is well known that the PSA concentration for a normal person ranges from 0 to 4 ng mL^{-1}. [5]

The conventional methods for cancer biomarker detection are enzyme-linked immunosorbent assay (ELISA), fluorescence, electrophoretic, chemiluminescence, and mass spectrometric immunoassays. However, these conventional methods take place at dedicated centralized laboratories using large, automated analyzers, requiring sample transportation, increased waiting times and increased administration and medical costs, so simple ways to provide affordable and reliable measurement are important. [4] Due to its inherent simplicity, low cost, high sensitivity, and miniaturization, the electrochemical immunoassay and immunosensor technique have attracted considerable interest. [6] Especially, sandwich-type immunoassay protocol is regarded as a more sensitive platform. [7] The sandwich type immunoassay with simple instrumentation and easy signal quantification is the predominant analytical technique for tumor markers detection.

In order to improve the amount of immobilization of biomolecules and enhance the sensitivity of the detection method, various signal amplification strategies have been developed, such as rolling circle amplification, enzyme labeling amplification, and polymerase chain reaction. [8] Among these strategies, nanomaterial-based

strategies have potential in realizing ultrasensitive biological detection due to the versatile properties of nanomaterials. [9] Based on this concept, many researchers choose some carbon materials such as carbon nanotubes, [4,8,10] carbon nanohorns, [11] graphene, [12-14] mesoporous carbons, [15,16] and fullerene [17] as efficient carriers. Among these carbon materials, mesoporous carbon is an excellent material for applications in catalysis, sensing and energy storage due to its unique features, such as good electrical conductivity, good biocompatibility, excellent adsorption properties, large specific surface area, high pore volume, and tunable porosity. [16] In addition, mesoporous materials with excellent performances are especially desirable for efficient immobilization of biomolecules. [9] Among mesoporous carbon materials, CMK-3 has attracted much attention because of its highly ordered 2D hexagonal structure with excellent textural characteristics. [18]

Enzyme labeling amplification has been widely used during the past few decades because of its high selectivity and sensitivity. However, the practical applications of such a natural enzyme-based strategy are limited due to complicated immobilization procedures, especially environmental instability, and high cost. To overcome these limitations, a lot of nanomaterials such as noble metal, metal oxide, and noble metal@metal oxide nanostructures have been explored as additional electrochemical catalysts or artificial mimetic enzymes to fabricate more sensitive electrochemical immunosensors. [8,19-24] Nanostructured metal oxide semiconductors possesses high surface area, nontoxicity, good biocompatibility, sensitivity, and chemical stability that can easily be modified for immobilization of biomolecules for biosensor

applications. [25] As a kind of metal oxide nanomaterials, flower-like SnO_2 nanostructures with desirable properties such as good chemical stability, high catalytic activity, low cost, and environmental friendliness have been reported. [26] However, electrochemical immunosensors based on flower-like SnO_2 have received little attention.

It has been reported that some metal NPs including platinum NPs, gold NPs, silver NPs, and palladium NPs exhibit intrinsic peroxidase-like activity, [9] providing promising opportunities for the development of the signal amplification strategy. Among these metal NPs, palladium NPs are considered as one of the most promising candidates because of their lower cost and superior catalytic activity. [27] Moreover, noble metals with ultrafine sizes have attracted substantial attention because their large surface areas and high number of edge and corner atoms significantly enhance the catalytic properties of noble metal nanocomposites. However, surface energies increase with decreasing noble metal particle size, leading to serious aggregation of small particles. To overcome this aggregation, the metal particles must be anchored to suitable supports. Thus, the flower-like nanostructures of SnO_2 could provide a large specific surface area, potentially making them excellent candidates for the growth and anchorage of numerous palladium NPs. Therefore, the Pd@flower-like SnO_2 nanocomposites as natural peroxidase mimics were fabricated in this work for signal amplification. The synthesis of excellent noble metal@metal oxide nanomaterials as electrochemical catalysts or peroxidase mimicking enzymes is an important issue. Thus, in the present work, we synthesized highly dispersed palladium@flower-like tin

dioxide (Pd@flower-like SnO_2) and gold@mesoporous carbon (Au@CMK-3) nanomaterials. In addition, to achieve further signal amplification based on enzymatic catalytic reactions, enzyme, such as horseradish peroxidase (HRP), has been widely used in the fields of electrochemical immunosensors. [9]

Herein, the proposed electrochemical immunosensor for PSA detection approach is expected to be highly sensitive due to the use of the Au@CMK-3 nanocomposite as a nanocarrier, Au/Pd@flower-like SnO_2 nanocomposite as platform, the ultrafine Pd NPs supported on flower-like SnO_2 as an electrocatalyst, and signal amplification based on HRP enzymatic reactions. Firstly, flower-like SnO_2 was synthesized by the hydrothermal method without using any capping agent. Monodispersed ultrafine palladium nanoparticles (Pd NPs) with a uniform size of ~3.5 nm were successfully anchored on the flower-like SnO_2 surface via a chemical reduction method. Au NPs were subsequently electrodeposited onto the surface of Pd@flower-like SnO_2 nanocomposite for immobilizing plentiful of the primary antibodies (Ab1). Secondly, uniform and highly dispersed Au NPs were anchored onto CMK-3 via a chemical reduction method to obtain the Au@CMK-3 nanocomposite with large surface areas and more active sites, which was used as nanocarriers for highly dense immobilization of redox-active probe methylene blue (MB), secondary antibodies (Ab2), and HRP molecules. In addition, the ultrafine Pd NPs supported on flower-like SnO_2 exhibit intrinsic peroxidase-like activity in the presence of H_2O_2, allowing significant amplification of the electrochemical signal and improving the sensitivity of the PSA immunosensor. Moreover, signal amplification was further enhanced by the

133 excellent electrocatalytic activity of abundant HRP immobilized on Au@CMK-3.
134 Thus, the proposed immunosensor showed high sensitivity for quantitative PSA
135 detection. As illustrated in **Scheme 1**, the proposed protocol for monitoring PSA
136 involves the preparation of a secondary Au@CMK-3-MB-Ab2-HRP bioconjugate
137 (Ab2 bioconjugate), the stepwise modification of the proposed PSA immunosensor,
138 and the principle of the electrochemical signal amplification.
139

140 **2. Materials and methods**

141 **2.1. Chemicals and materials**

142 Anti-PSA antibodies, PSA, and free PSA (f-PSA) were purchased from Biocell Co.
143 (Zhengzhou, China). CMK-3 (specific surface area, pore diameter, and pore volume
144 are 1431 $m^2 g^{-1}$, 3.8 nm, and 1.51 $cm^3 g^{-1}$, respectively) was purchased from Nanjing
145 XFNANO Materials Tech Co., Ltd. (Nanjing, China). $HAuCl_4$, $PdCl_2$, and HRP were
146 obtained from Sigma Chemical Co. (St. Louis, MO, USA). OVA was purified from
147 egg in our laboratory. [28] All other reagents were of analytical grade. Phosphate buffer
148 (PBS, 0.1 M, pH 7.0) was used as working solution. All aqueous solutions were
149 prepared with deionized water (DW, 18 MΩ cm).
150

151 **2.2. Synthesis of flower-like SnO_2 nanocrystals**

152 Flower-like SnO_2 nanostructures were synthesized by the hydrothermal method
153 according to the method of Zhang et al. [26] with minor modification. In a typical
154 reaction: 1.296 g NaOH, 1.052 g $SnCl_4 \cdot 5H_2O$, 0.68 g $Na_2SO_4 \cdot 5H_2O$ and 40 mL of

DW were put in a beaker. After stirring for about 5 min, 40 mL of absolute ethanol was added into the reaction mixture to obtain a white translucent suspended solution, which was then transferred into a 100 mL Teflon-lined autoclave. The vessel was sealed and put in a furnace preheated to 180 ^{o}C. After reacting for 24 h, the vessel was taken out and let cool down to room temperature naturally. The blue product was washed with DW and ethanol for three times.

2.3. Synthesis of Pd@flower-like SnO_2 nanohybrid

The Pd@flower-like SnO_2 nanohybrid was prepared as follows: flower-like SnO_2 (30.0 mg), polyethylene glycol 400 (0.1 mL), sodium citrate (0.01 M, 1.0 mL), and $PdCl_2$ aqueous solution (0.01 M, 0.5 mL) were dispersed into 10.0 mL of DW via sonication, and then the mixture was stirred with a magnetic stirrer for 0.5 h at room temperature. Three milliliter of 15.0 mM sodium borohydride solution was added dropwise and stirred for 0.5 h and shaken for an additional 3.5 h. After centrifuging and washing with DW for three times, the resulting Pd@flower-like SnO_2 nanohybrid was obtained by freeze-drying.

2.4. Synthesis of Au@CMK-3 nanohybrid

The Au@CMK-3 nanohybrid was prepared as follows: CMK-3 (10.0 mg), polyethylene glycol 400 (0.1 mL), sodium citrate (0.01 M, 1.0 mL), and $HAuCl_4$ aqueous solution (0.01 M, 0.25 mL) were dispersed into 5.0 mL of DW via sonication, and then the mixture was stirred with a magnetic stirrer for 0.5 h at room temperature.

Two milliliter of 25.0 mM ascorbic acid solution was added dropwise and stirred for 0.5 h and shaken for an additional 2.0 h. After centrifuging and washing with DW for three times, the resulting Au@CMK-3 nanohybrid was obtained by freeze-drying.

2.5. Materials characterizations

The morphologies of the prepared samples were characterized by a QUNT200 scanning electron microscopy (SEM, USA) equipped with an energy dispersive X-ray spectrometry (EDX) and a JEM 2100 transmission electron microscopy (TEM, Japan). X-ray diffraction spectra were obtained by using a Rigaku TTR III X-ray diffractometer (XRD, Japan).

2.6. Preparation of Au@CMK-3-MB-Ab2-HRP bioconjugate (Ab2 bioconjugate)

Initially, 2.0 mL of 1.0 mg mL^{-1} MB aqueous solutions were added into 5.0 mL of 1.0 mg mL^{-1} Au@CMK-3 aqueous solutions and stirred at 4 ^{o}C for 24 h. After excess MB was removed by centrifugation and washing with DW three times, the resulting Au@CMK-3-MB nanocomposite was re-dispersed in 2.0 mL of 0.1 M pH 7.0 PBS and stored at 4 ^{o}C before use. Secondly, 100 μL of 1.0 mg mL^{-1} anti-PSA was added dropwise into the Au@CMK-3-MB mixture under continuous stirring gently at 4 ^{o}C for 12 h. Thirdly, 100 μL of 1.0 mg mL^{-1} HRP was then added into the above mixture and stirred for another 12 h. Finally, the Au@CMK-3-MB-Ab2-HRP bioconjugate was obtained by further centrifugation and re-dispersed in 1.0 mL pH 7.0 PBS for further use. All the above experiments were performed at 4 ºC.

199

200 **2.7. Fabrication process of the immunosensor**

201 Prior to the preparation procedure, glassy carbon electrode (GCE, 3 mm in
202 diameter) was polished with 0.3 and 0.05 μm Al_2O_3 powder respectively and
203 subsequently sonicated in ethanol and DW to remove the physically adsorbed
204 substance and dried at in air. To prepare the Pd@SnO_2 modified electrode, 6 μL of 1.0
205 mg mL^{-1} Pd@flower-like SnO_2 dispersed by aqueous solution was dropped onto the
206 electrode surface and dried at room temperature. In order to capture the primary Ab1,
207 Au NPs were electrodeposited on the surface of the Pd@SnO_2 modified electrode in
208 0.5 mM $HAuCl_4$ aqueous solution under the potential –0.2 V for 400 s. Subsequently,
209 the Au-Pd@SnO_2 modified electrode was submerged into a solution of 10 μg mL^{-1}
210 anti-PSA (Ab1) at 4 ^oC for 12 h to yield Ab1/Au/Pd@SnO_2/GCE. Finally, to block
211 possible remaining active sites and eliminate the risk of nonspecific binding, 0.25
212 wt% OVA dissolved by 0.1 M pH 7.0 PBS was coated on the electrode and incubated
213 for 40 min at room temperature. Ultimately, the OVA/Ab1/Au/Pd@SnO_2 modified
214 GCE was obtained and stored at 4 ºC when not in use. After each modification step,
215 the modified electrode was cleaned with 0.1 M pH 7.0 PBS to remove the physically
216 absorbed species. The stepwise assembly of the proposed immunosensor is illustrated
217 in **Scheme 1**.

218

219 **2.8. Electrochemical measurements**

220 Differential pulse voltammetry (DPV) and electrochemical impedance

spectroscopy (EIS) experiments were performed with a CHI 660E Electrochemical Workstation from Shanghai Chenhua Instrument (Shanghai, China) and conducted using a three-electrode system, with the modified GCE as working electrode, a platinum wire as the counter electrode, a saturated calomel electrode as the reference electrode. All the measurements were carried out at room temperature. Based on sandwich-type immunoassay format, the immunosensor was first incubated with 20 μL PSA with various concentrations in 0.1 M pH 7.0 PBS for 1 h at room temperature, then incubated with 20 μL Ab2 bioconjugates for another 1.0 h at room temperature. Each assembling procedure was followed by a careful rinse to remove excess materials in the electrode surface. DPV response was recorded in 0.1 M pH 7.0 PBS containing 2.0 mM H_2O_2 with a potential range of 0.1 to –0.6 V, modulation amplitude of 0.05 V, pulse width of 0.05 s, and sample width of 0.0167s. Additionally, electrochemical characterization of the immunosensor using DPV and EIS investigation were performed in 0.1 M pH 7.0 PBS containing 2 mM $[Fe(CN)_6]^{3-/4-}$ and 0.1 M KCl. DPV responses were recorded in the potential range of 0.5 to –0.1 V with a pulse amplitude of 0.05 V and a pulse width of 0.05 s, and sample width of 0.0167s. EIS was tested at the potential of 0.1 V in the frequency range of $10^{-1} \sim 10^5$ Hz with an amplitude of 5 mV.

3. Results and discussion

3.1. Characterization of Au-Pd@flower-like SnO_2 and Au@CMK-3

The morphologies and microstructures of flower-like SnO_2 and Pd@flower-like

243 SnO_2 were investigated by SEM and TEM observation. **Fig. 1A** illustrates typical
244 SEM image of the synthesized flower-like SnO_2, indicating the flower-shaped
245 structure like snow cone with size of approximately 3 μm consisting of dense SnO_2
246 nanorods with typical length around 1 μm and diameter of 200 nm. The unique
247 morphology of Pd@flower-like SnO_2 is also characterized by TEM and HR-TEM for
248 100,000 and 800,000 magnification as illustrated in **Fig. 1B and C**, respectively. The
249 most striking feature is that the Pd NPs with a uniform size ~3.5 nm are fairly well
250 monodispersed on the surface of flower-like SnO_2. It should be noted that the
251 ultradispersed and ultrafine Pd NPs supported on flower-like SnO_2 may be favorable
252 for the reduction of H_2O_2 due to its excellent and intrinsic peroxidase-like
253 electrocatalytic activity. [9] The crystal structures of flower-like SnO_2 and
254 Pd@flower-like SnO_2 were investigated through XRD, as shown in **Fig. S1**. All the
255 peaks can be indexed to the tetragonal phase of SnO_2 (JCPDS 41-1445), and no peaks
256 of impurities are detected, indicating that the SnO_2 samples are pure and well
257 crystallized. [26] The major diffracted peaks of Pd@flower-like SnO_2 are the same as
258 those of as-prepared SnO_2. The sharp diffraction peaks from both samples suggest a
259 high crystallinity of our synthesized Pd@flower-like SnO_2 and SnO_2 nanocrystals.
260 However, it should be noted that no peaks attributed to Pd are detected, which might
261 be due to the low amount. [29, 30] The Pd loading is determined by ICP: 1.6 wt% in our
262 study. Lower Pd loading is usually adopted because Pd is a noble metal of high cost.
263 The EDX analysis of Au-Pd@flower-like SnO_2 nanocomposites were obtained as
264 illustrated in **Fig. 1D**. It can be clearly noticed that the Pd and Au loading are 1.39

wt% and 3.41 wt%, respectively. The 15.85 wt% C element is detected by the EDX analysis, which must be the carbon element in the electrode. Thus, the real Pd and Au loading should be 1.65 wt% and 4.05 wt% when the carbon element was excluded. It is clear to find that the Pd loading determined by ICP is approximately in accordance with the results of EDX and XRD. Besides, we can also conclude that 4.05 wt% Au NPs were electrodeposited onto the surface of Pd@flower-like SnO_2 nanocomposites. TEM images of Au@CMK-3 at different magnifications (E for 15,000 magnification and F for 100,000 magnification) were also obtained as shown in **Fig. 1E and F**. It is interesting to notice that uniform and highly dispersed Au NPs were anchored onto CMK-3. The uniform and highly dispersed Au NPs on the surface of CMK-3 are very useful for immobilization of large amount of secondary antibodies and HRP molecules, which are especially important for the successful formation of the Ab2 bioconjugate in this assay. Also, the ordered mesoporous structure of the CMK-3 could be clearly observed from **Fig. 1F**, which is responsible for the adsorption of large amounts of redox-active probe MB.

3.2. Feasibility of the immunosensor

The feasibility of the proposed PSA immunosensor was explored with different modified surfaces by DPV responses for 10 ng mL^{-1} PSA. As can be seen from **Fig. 2A**, almost no detectable electrochemical signal is observed for the immunosensor incubated with PSA (curve a) due to the absence of the redox mediator MB. The capture of the secondary Au@CMK-3-MB-Ab2-HRP bioconjugate caused an increase

in current response because of the formation of the immunoreaction complex and attachment of redox-active probe MB (curve b). A considerable increase in current response (curve c) was observed after addition of 2.0 mM H_2O_2 in 0.1 M pH 7.0 PBS since the catalytic ability of ultrafine Pd NPs supported on flower-like SnO_2 and large amount of HRP in Ab2 bioconjugate greatly enhanced the typical electrocatalysis of H_2O_2 reduction. These results clearly indicate the dramatic signal amplification capability of our proposed strategy.

3.3. Electrochemical characterization of immunosensor

DPV and EIS which can indicate the change of surface area, resistance and carried charge could provide additional information about electrode surface modification. Thus, the assembly process of modified electrode could be monitored using DPV and EIS techniques. **Fig. 2B** represents the DPV of different modified electrodes during the stepwise fabrication. The bare GCE exhibited an reduction peak **(curve a)** of ferricyanide ions. When Pd@SnO_2 composite was modified on the GCE, an increased peak current **(curve b)** was obtained, as a result of the high surface area the flower-like SnO_2 for improving the effective area of electrode and the high conductivity of Pd NPs for facilitation of electron transfer. After electrodeposition of Au NPs, the peak current response **(curve c)** increased drastically. The significantly enhanced current response could be attributed to the fact that Au NPs with excellent conductivity and large surface area could amplify the electrochemical signal. When anti-PSA (Ab1) was assembled onto the electrode via Au-S affinity, there was an

obvious decrease of the current response **(curve d)**, which suggested that large amount of antibody had been successfully immobilized on the electrode surface. The reason for the decrease of the current response is that anti-PSA as protein biomacromolecules hindered the tunnel of electron shuttle. Non-conductive OVA as the blocking agent made the peak current decrease again **(curve e)**. The incubation of PSA (10 ng mL^{-1}) led to further decrease of peak current **(curve f)**, attributing to the formation of immunocomplex on electrode surface which increased steric hindrance and blocked electron transfer. Inspiringly, the incubation of the Ab2 bioconjugate increased the peak current of the immunosensor remarkably **(curve g)**. The reason might be attributed to the fact that the CMK-3 possess high surface areas and mesoporous structure, which can absorb abundant of ferricyanide ions on the aurface of the electrode. Additionally, the Au@CMk-3 composites have high conductivity and good electron transfer efficiency, which facilitated the electron communication between the solution and the base electrode. Moreover, EIS has been proven to be one of the most powerful tools for characterizing the interface properties of the modified immunosensors. The impedance spectra include a semicircle portion and a linear portion. The semicircle portion at higher frequencies corresponds to the electron-transfer limited process, and the linear portion at lower frequencies represents the diffusion-limited process. The semicircle diameter equals the electron-transfer resistance. **Fig. 2C** shows the Nyquist diagrams of EIS upon the stepwise modification process. It was observed that the EIS of Pd@SnO_2 composite modified electrode **(curve b)** decreased compared with the bare GCE **(curve a)**,

indicating that the synthesized Pd@flower-like SnO_2 composite had a high electronic conductivity, and favored for electron communication between the solution and the electrode. After Au NPs were electrodeposited of on Pd@flower-like SnO_2 composite, a much lower resistance **(curve c)** was obtained than the former, suggesting that Au NPs was highly beneficial to the electron transfer. However, when the electrode was conjugated with Ab1, the resistance increased obviously **(curve d)**, which suggested that the Ab1 was successfully immobilized on the surface and formed an additional barrier and blocked the electron exchange between the redox probe and the electrode. After OVA was immobilized onto the electrode surface, the resistance increased again **(curve e)**, which was caused by the nonconductive properties of biomacromolecule. Then, the resistance increased further **(curve f)** when PSA was recognized onto the electrode, indicating that the formed immunocomplex blocked the electron transfer. At last, when the secondary Au@CMK-3-MB-Ab2-HRP bioconjugate interacted with PSA **(curve g)**, interestingly the resistance decreased significantly, indicating that the synthesized Au@CMK-3-MB-Ab2-HRP bioconjugate possess high conductivity and good electron transfer efficiency, although the protein adsorption layer acted as barrier to the interfacial electron transfer. The EIS results were in accordance with those obtained from DPV measurements as mentioned above, which demonstrated the successful fabrication of the immunosensor.

3.4. Calibration curve of immunosensor

Under optimized experimental conditions, the analytical performance of the

353 proposed immunosensor incubated with different concentrations of PSA was assessed
354 using DPV in 0.1 M pH 7.0 PBS containing 2.0 mM H_2O_2. Usually, the Pd NP with
355 peroxidase-like activity was located on the Ab2 conjugate in some electrochemical
356 immunosensors. However, in this work, it was supported on flower-like SnO_2 and
357 used as platform as this approach is relatively uncomplicated although it caused a
358 little bit of background current. Similar work was also reported as the HRP was
359 located on the platform. [9] From **Fig. 2D**, it can be seen that DPV peaks exhibited clear
360 dependence on the concentrations of target PSA because elevated PSA concentrations
361 from 0.01 to 100 ng mL^{-1} led to increases in current responses, which suggested the
362 capture of more secondary Ab2 bioconjugate and abundant immobilization of the
363 redox mediator MB on the electrode surface. As shown in **Fig. 2E**, the resulting
364 calibration plots displayed a good linear relationship between the current response and
365 the logarithm of PSA concentration ranging from 0.01 to 100 ng mL^{-1}, and a detection
366 limit of 3 pg mL^{-1} could be estimated using the 3σ rule. The corresponding regression
367 equation was I (μA) = –9.82 log*c* – 28.38 with a correlation coefficient of 0.9983.
368 Compared with other sensors reported previously, the proposed immunosensor
369 exhibited a satisfactory detection limit and linear range. The characteristics of other
370 PSA sensors are summarized in **Table 1**. It revealed that the proposed PSA
371 immunosensor exhibited high sensitivity, which was attributed to both the
372 electrocatalysis of ultrafine Pd NPs supported on flower-like SnO_2 and abundant HRP
373 in Ab2 bioconjugate toward H_2O_2 reduction, and high loading of redox-active probe
374 MB based on CMK-3 with large surface areas and mesoporous structure.

3.5. Selectivity, reproducibility, and stability

The selectivity of the proposed immunosensor was evaluated by challenging it against other potential interferents in 0.1 M pH 7.0 PBS with 2.0 mM H_2O_2, and the results are shown in **Fig. 2F**. As can be seen, with an excess (100-fold) amount of nontarget analytes, PSA (1 ng mL^{-1}) against BSA (100 ng mL^{-1}), glucose (100 ng mL^{-1}), f-PSA (100 ng mL^{-1}), dramatic increases in DPV response of 1 ng mL^{-1} PSA were observed. Moreover, the presence of a mixture of 1 ng mL^{-1} PSA and the tested interferents led to the same dramatic increase in current response. This revealed the high specificity of the proposed electrochemical immunosensor. The reproducibility of the present immunosensor was examined by using five equally modified electrodes to detect 1 ng mL^{-1} PSA. The reproducible electrochemical signals were produced with a relative standard deviation of 4.5%, indicating a good reproducibility of our protocol. Successive cyclic potential scans for 50 cycles and long-term storage assay were used to examine the stability of the proposed immunosensor. A 6.2% decrease of initial peak current was found after 50 continuous cycle scans. Additionally, the long-term stability experiment was carried out intermittently (every 5 days). When the immunosensor was not in use, it was stored in a refrigerator at 4 ^{o}C. Over 96.3% and 89.5% of initial response remained after storage of 15 and 30 days, respectively. The acceptable stability of the immunosensor may be ascribed the good chemical stability, biocompatibility, and nontoxicity of the Au-Pd@flower-like SnO_2 nanocomposites.

3.6. Real sample analysis

In order to evaluate the feasibility of the proposed immunosensor for real sample analysis, the immunosensor was used for the determination of PSA by standard addition methods in serum samples. A series of PSA standard solutions with various concentrations was injected to 10-fold-diluted human serum samples, and DPV measurements of the resulting solutions were subsequently recorded. **Table 2** presents the experimental results with recoveries from 97.2% to 106.0% and RSDs from 3.2% to 6.5%. Therefore the proposed electrochemical immunosenor showed potential as an effective tool for specific PSA diagnostics in real samples. As the PSA concentration for a normal person ranges from 0 to 4 ng mL^{-1}, the detection limit (3 pg mL^{-1}) and linear range (0.01 to 100 ng mL^{-1}) obtained by the present work is able to determine PSA in human serum samples, implying potential applications in immunoassays.

4. Conclusion

In summary, we have successfully developed a novel electrochemical immunosenor for PSA detection based on Au/Pd@flower-like SnO_2 as sensing platform and Au@CMK-3 as nanocarriers for signal amplification . The employment of Au@CMK-3 as nanocarriers led to attachment of large amounts of redox-active probe MB on the electrode surface. A remarkable signal amplification strategy was achieved based on the electrocatalysis of monodispersed ultrafine Pd NPs supported on flower-like SnO_2 and abundant HRP immobilized on Au@CMK-3 toward H_2O_2 reduction, which resulted in an improved detection limit. In view of these advantages,

419 the electrochemical sensing platform is thus expected to provide new insights for
420 other biomarkers in clinical diagnosis.
421
422 **Acknowledgments**
423 This work was supported by the National Natural Science Foundation of China
424 (31160334) and the Natural Science Foundation of Yunnan Province (2012FB112,
425 2014RA022), People's Republic of China.
426
427 **References:**
428 1 H. D. Jang, S. K. Kim, H. Chang, J. W. Choi, *Biosens. Bioelectron.*, 2015, **63**,
429 546–551.
430 2 B. Zhang, B. Liu, G. Chen, D. Tang, *Biosens. Bioelectron.*, 2015, **64**, 6–12.
431 3 L. Ding, J. You, R. Kong, F. Qu, *Anal. Chim. Acta*, 2013, **793**, 19–25.
432 4 B. Kavosi, A. Salimi, R. Hallaj, K. Amani, *Biosens. Bioelectron.*, 2014, **52**,
433 20–28.
434 5 M. Yang, A. Javadi, H. Li, S. Gong, *Biosens. Bioelectron.*, 2010, **26**, 560–565.
435 6 F. Yang, Z. Yang, Y. Zhuo, Y. Chai, R. Yuan, *Biosens. Bioelectron.*, 2015, **66**,
436 356–362.
437 7 H. Fan, Z. Guo, L. Gao, Y. Zhang, D. Fan, G. Ji, B. Du, Q. Wei, *Biosens.*
438 *Bioelectron.*, 2015, **64**, 51–56.
439 8 W. Xu, S. Xue, H. Yi, P. Jing, Y. Chai, R. Yuan, *Chem. Commun.*, 2015, **51**,
440 1472–1474.

9 W. Xu, Y. Wu, H. Yi, L. Bai, Y. Chai, R. Yuan, *Chem. Commun.*, 2014, **50**, 1451–1453.

10 R. Das, S. Upadhyay, M. K. Sharma, M. Shaik, V. K. Rao, D. N. Srivastav, *RSC Adv.*, 2015, **5**, 48147–48153.

11 F. Yang, J. Han, Y. Zhuo, Z. Yang, Y. Chai, R. Yuan, *Biosens. Bioelectron.*, 2014, **55**, 360–365.

12 R. Zhang, B. Pan, H. Wang, J. Dan, C. Hong, H. Li, *RSC Adv.*, 2015, **5**, 38176–38182.

13 K. Shang, X. Wang, B. Sun, Z. Cheng, S. Ai, *Biosens. Bioelectron.*, 2013, **45**, 40–45.

14 G. Sun, J. Lu, S. Ge, X. Song, J. Yu, M. Yan, J. Huang, *Anal. Chim. Acta*, 2013, **775**, 85–92.

15 H. Fan, Y. Zhang, D. Wu, H. Ma, X. Li, Y. Li, H. Wang, H. Li, B. Du, Q. Wei, *Anal. Chim. Acta*, 2013, **770**, 62–67.

16 D. Wu, A. Guo, Z. Guo, L. Xie, Q. Wei, B. Du, *Biosens. Bioelectron.*, 2014, **54**, 634–639.

17 H. Wang, J. Zhang, Y. Yuan, Y. Chai, R. Yuan, *RSC Adv.*, 2015, **5**, 58019–58023.

18 B. Kuppan, P. Selvam, *Prog. Nat. Sci.*, 2012, **22**, 616–623.

19 A. Guo, Y. Li, W. Cao, X. Meng, D. Wu, Q. Wei, B. Du, *Biosens. Bioelectron.*, 2015, **63**, 39–46.

20 L. Li, J. Xu, X. Zheng, C. Ma, X. Song, S. Ge, J. Yu, M. Yan, *Biosens. Bioelectron.*, 2014, **61**, 76–82.

21 X. Sun, Z. Ma, *Anal. Chim. Acta*, 2013, **780**, 95–100.

22 X. Wang, L. Chen, X. Su, S. Ai, *Biosens. Bioelectron.*, 2013, **47**, 171–177.

23 J. Gao, Z. Guo, F. Su, L. Gao, X. Pang, W. Cao, B. Du, Q. Wei, *Biosens. Bioelectron.*, 2015, **63**, 465–471.

24 Y. Liu, T. Yan, Y. Li, W. Cao, X. Pang, D. Wu, Q. Wei, *RSC Adv.*, 2015, **5**, 19581–19586.

25 N. Lavanya, S. Radhakrishnan, C. Sekar, *Biosens. Bioelectron.*, 2012, **36**, 41–47.

26 H. Zhang, C. Hu, X. He, L. Hong, G. Du, Y. Zhang, *J. Power Sources*, 2011, **196**, 4499–4505.

27 L. Yang, H. Zhao, S. Fan, B. Li, C.-P. Li, *Anal. Chim. Acta*, 2014, **852**, 28–36.

28 C.-P. Li, Z. K. He, X. Y. Wang, L. Yang, C. Y. Yin, N. Zhang, J. Lin, H. Zhao, *Food Chem.*, 2014, **148**, 209–217.

29 L. B. Yang, X. Jiang, W. D. Ruan, J. X. Yang, B. Zhao, W. Q. Xu, and J. R. Lombardi, *J. Phys. Chem. C*, 2009, **113**, 16226–16231.

30 H. Zhang, G. Wang, D. Chen, X. J. Lv, and J. H. Li, *Chem. Mater.*, 2008, **20**, 6543–6549.

31 A. Salimi, B. Kavosi, F. Fathi, R. Hallaj, *Biosens. Bioelectron.*, 2013, **42**, 439–446.

32 H. Wang, Y. Zhang, H. Yu, D. Wu, H. Ma, H. Li, B. Du, Q. Wei, *Anal. Biochem.*, 2013, **434**, 123–127.

33 J. Han, Y. Zhuo, Y. Chai, R. Yuan, W. Zhang, Q. Zhu, *Anal. Chim. Acta*, 2012, **746**, 70–76.

34 Y. Li, J. Han, R. Chen, X. Ren, Q. Wei, *Anal. Biochem.*, 2015, **469**, 76–82.

35 Y. Wan, W. Deng, Y. Su, X. Zhu, C. Peng, H. Hu, H. Peng, S. Song, C. Fan, *Biosens. Bioelectron.*, 2011, **30**, 93–99.

36 M. Yang, A. Javadi, S. Gong, *Sens. Actuators B*, 2011, **155**, 357–360.

Figure captions:

Scheme 1. Schematic diagram for the stepwise assembly procedure of the electrochemical immunosensor and the signal amplification strategy.

Fig. 1. SEM image of flower-like SnO_2 (A), TEM images of Pd@flower-like SnO_2 at different magnifications (B for 100000 magnification and C for 800000 magnification), EDX analysis of Au/Pd@flower-like SnO_2 (D), TEM images of Au@CMK-3 at different magnifications (E for 15000 magnification and F for 100000 magnification).

Fig. 2. (A) DPV curves of the proposed immunosensor incubated with (a) 10 ng mL^{-1} PSA and (b) Ab2 bioconjugates in 0.1 M pH 7.0 PBS, and with (c) Ab2 bioconjugates in 0.1 M pH 7.0 PBS containing 2.0 mM H_2O_2. DPV measurements were carried out by scanning the potential from 0.1 to –0.6 V with an amplitude of 0.05 V, a pulse width of 0.05 s, and a sample width of 0.0167s. DPV (B) and EIS (C) characterization of different modified electrode (a) bare GCE; (b) Pd@SnO_2/GCE; (c)

Au/Pd@SnO_2/GCE; (d) Ab1/Au/Pd@SnO_2/GCE; (e) OVA/Ab1/Au/Pd@SnO_2/GCE; (f) PSA/OVA/Ab1/Au/Pd@SnO_2/GCE; (g) Ab2 bioconjugate/PSA/OVA/Ab1/Au/Pd@SnO_2/GCE in 0.1 M pH 7.0 PBS containing 2.0 mM $[Fe(CN)_6]^{3-/4-}$ and 0.1 M KCl. DPV measurements were carried out by scanning the potential from 0.5 to –0.1 V with an amplitude of 0.05 V, a pulse width of 0.05 s, and sample width of 0.0167s. EIS was recorded in the frequency range of $10^{-1} \sim 10^{5}$ Hz with an amplitude of 5 mV. (D) DPV curves for different concentrations of target PSA for the proposed immunosensor in 0.1 M pH 7.0 PBS containing 2.0 mM H_2O_2. DPV measurements were carried out by scanning the potential from 0.1 to –0.6 V with an amplitude of 0.05 V, a pulse width of 0.05 s, and sample width of 0.0167s. (E) The resulting calibration plot for log[target PSA] *vs*. DPV response in the range of 0.01 to 100 ng mL^{-1}. Error bars: SD, n= 3. (F) Selectivity of the proposed immunosensor with BSA (100 ng mL^{-1}), glucose (100 ng mL^{-1}), f-PSA (100 ng mL^{-1}), PSA (1 ng mL^{-1}), and PSA (1 ng mL^{-1}) containing the above mixture of three interferents with the same concentrations.

Figures:

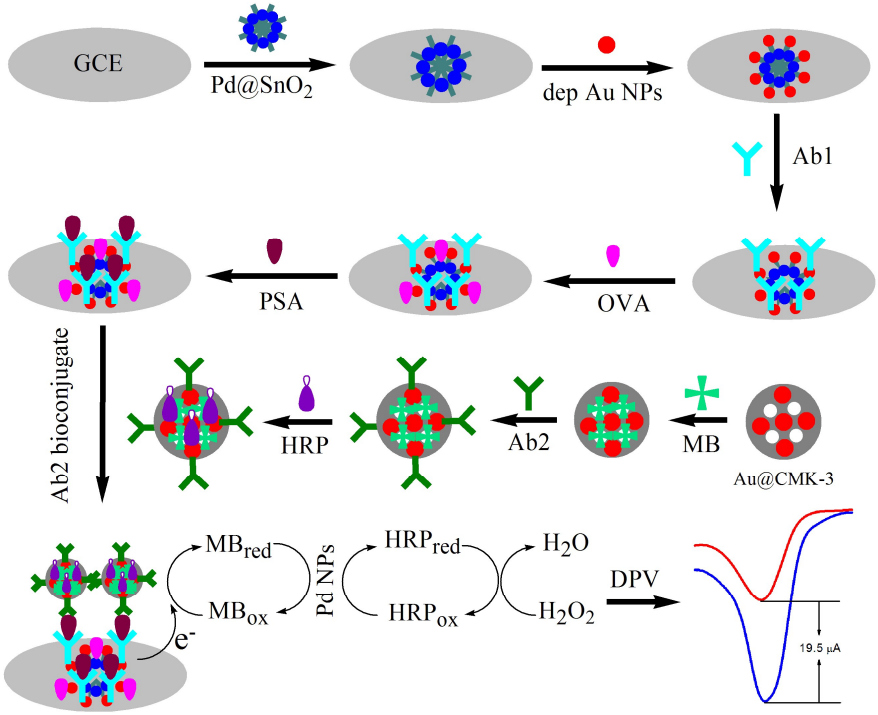

Scheme 1.

Yang et al.

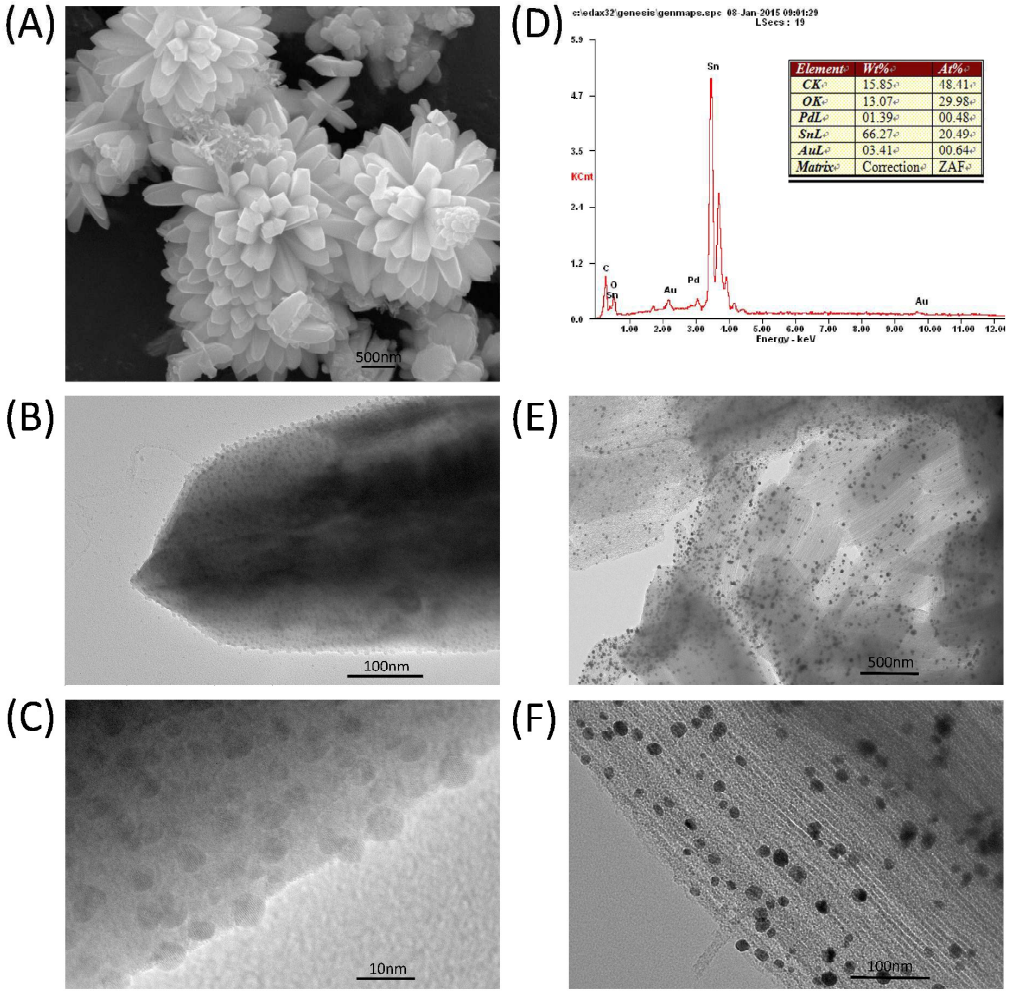

Fig. 1.

Yang et al.

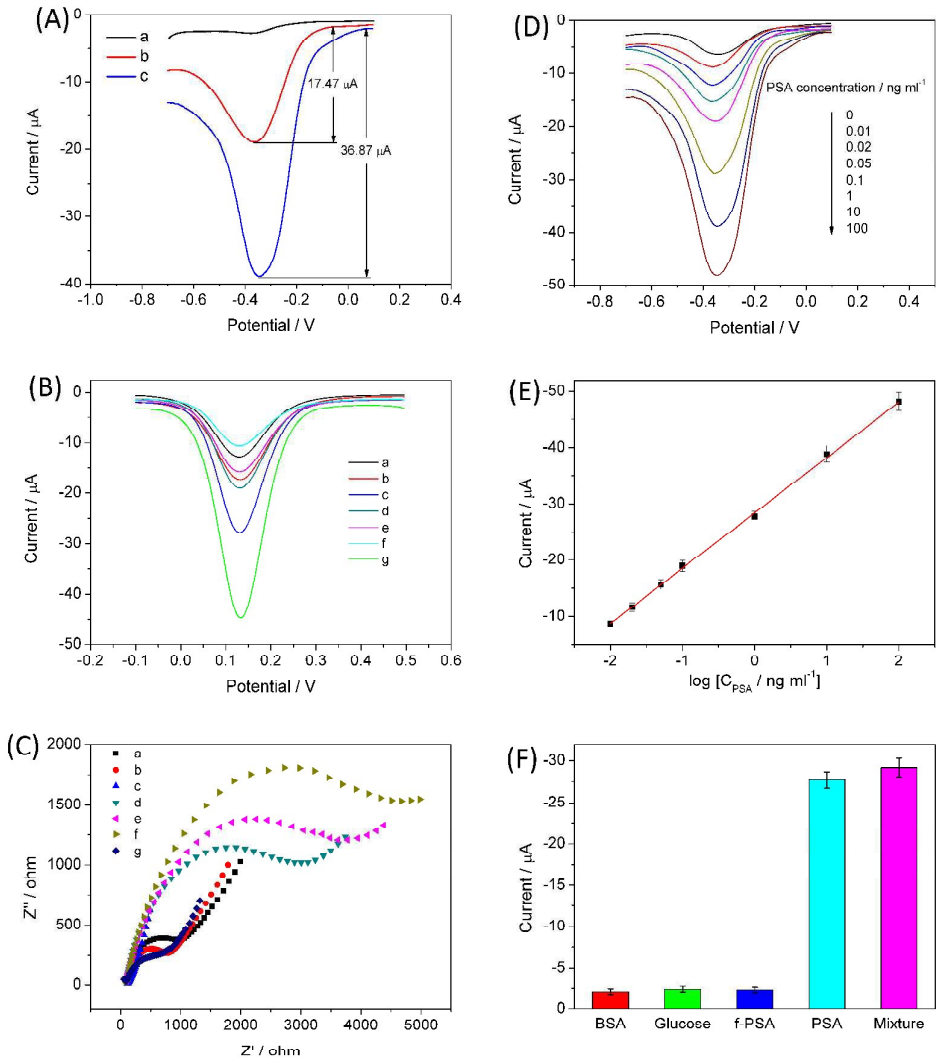

560

561

562

563

564

565

566

567 **Fig. 2.**

568 **Yang et al.**

569

570

Table 1

Comparison of different immunosensors for detection of PSA.

Electrode	Method	Liner range (ng mL^{-1})	LOD (ng mL^{-1})	Ref
Au-GR/GCE	CV	1.0–10	0.59	1
PS-Fc/GCE	SWV	0.01–20	0.001	3
Dendrimer/ILS/CNTs/GCE	DPV	0.05–80	0.001	4
MnO_2/Au/SPCE	DPV	0.005–100	0.0012	20
ILs/CNTs/GCE	DPV	0.2–40	0.02	31
AgNPs@MSNs/GCE	CV	0.05–50	0.015	32
AuNPs/PEI-PTCA/GCE	DPV	0.01–50	3.4	33
NH_2-GS@FCA/GCE	Amperometry	0.01–10	0.002	34
CNTs/SPCE	Amperometry	0.005–4	0.005	35
Quantum dot/GS/GCE	SWV	0.005–10	0.003	36
Au/Pd@flower-like SnO_2/GCE	DPV	0.01–100	0.003	This work

Table 2

Determination of PSA in human serum samples.

Sample	Added (ng mL^{-1})	Founded (ng mL^{-1})	RSD (%)	Recovery (%)
1	0.05	0.0486	5.7	97.2
2	1	0.988	6.5	98.8
3	5	5.18	5.1	103.6
4	10	10.6	4.2	106.0
5	30	29.2	3.2	97.3

Tables

Yang et al.